Supporting Information for:

Macro- and micro-spectroscopic study of Nd (III) uptake mechanisms in hardened cement paste

P.Mandaliev[a,b,*,**], R. Dähn[a], B. Wehrli[b,c], E. Wieland[a]

[a]*Laboratory for Waste Management, Paul Scherrer Institute, 5232 Villigen PSI, Switzerland*

[b]*Departement of Environmental Sciences, Swiss Federal Institute of Technology (ETH), 8092 Zürich, Switzerland*

[c]*Swiss Federal Institute for Environmental Science and Technology (EAWAG), 6047 Kastanienbaum, Switzerland*

For submission to Environmental Science and Technology

*Corresponding author
Phone: +41-56-56-310-5443
Fax: +41-56-310-3565
E-Mail: Peter.Mandaliev@psi.ch

**present address: Laboratory for Solid State Chemistry and Catalysis, Swiss Federal Laboratories for Materials Testing and Research (EMPA), 8600 Dübendorf, Switzerland;
Phone: +41-44-823-4340
Petar.Mandaliev@empa.ch

Coauthors:
E-Mail: rainer.daehn@psi.ch; bernhard.wehrli@eawag.ch; erich.wieland@psi.ch;

Pages 13

Tables 2

Figures 3

References

Materials and methods

TableS1: Chemical conditions of the Nd cement-sample preparation for μ-XAS measurements

Material (hydrated cement)	Abbreviation	Nd loading (μmol Nd / g solid)	Hydration time (days)	Method
Sample 1	CEMHYD-15M-26	26	15 min.	bulk-XAS
Sample 2	CEMHYD-1-26	26	1	bulk-XAS
Sample 3	CEMHYD-28-26	26	28	bulk-XAS
Sample 4	CEMHYD-200-26	26	200	bulk-XAS
Sample 5	CEMSORB-1-26	26	1	bulk-XAS
Sample 6	CEMSORB-28-26	26	28	bulk-XAS
Portlandite	PORTSORB-1-26	26	1	bulk-XAS
Sample 8				
ROI 1	CEMHYD-28-26-ROI-1	26	28	μ-XAS
ROI 2	CEMHYD-28-26-ROI-2	26	28	
ROI 3	CEMHYD-28-26-ROI-3	26	28	
ROI 4	CEMHYD-28-26-ROI-4	26	28	
ROI 5	CEMHYD-28-26-ROI-5	26	28	
ROI 6	CEMHYD-28-26-ROI-6	26	28	
ROI 7	CEMHYD-28-26-ROI-7	26	28	
ROI 8	CEMHYD-28-26-ROI-8	26	28	
ROI 9	CEMHYD-28-26-ROI-8	26	28	
Sample 9				
ROI 1	CEMHYD-200-26-ROI-1	26	200	μ-XAS
ROI 2	CEMHYD-200-26-ROI-2	26	200	
ROI 3	CEMHYD-200-26-ROI-3	26	200	

Details of the μ-XRF, bulk / μ-XAS data reduction

Higher harmonics of the primary energy were suppressed by a Si reflecting strip on a vertical focusing mirror after the monochromator (DUBBLE beamline at ESRF) and by detuning from the maximum incident intensity (beamline 10.3.2 at ALS). Reduction and modelling of the XAS data was performed with the ATHENA/ARTEMIS package *(1, 2)*. After background subtraction, the energy was converted to photoelectron wave vector units ($Å^{-1}$) by assigning the ionization energy of the Nd L_{III}-edge (6208 eV), E_0, to the first inflection point of the absorption edge. Radial structure functions (RSFs) were obtained by Fourier transforming k^3-weighted χ (k) functions in the range 1.4 - 10.6 $Å^{-1}$ using the Kaiser-Bessel window function with a smoothing parameter of 4. Single-shell fits were performed in real space across the range of the first and second coordination shell (ΔR = 1.25 – 4.0 Å) to determine the coordination number, *N*, the bond length, *R*, and the Debye-Waller (DW) factor, σ^2, using the amplitude reduction factor, S_0^2, fixed at 1.0 to correctly reproduce the number of neighboring atoms in the structural reference. Note that S_0^2 = 1.0 agrees with earlier studies of Nd coordination in water *(3)*. The interatomic distances, coordination numbers, and DW factors were allowed to vary in the single-shell analysis. In a subsequent step multi-shell fits were performed by using the estimated data from the single-shell analysis. The fitting parameters were treated as in the first shell fits except that σ^2 was fixed for the second shell using the data from the single-shell fits. The latter was necessary due to strong correlation of the Si and Ca backscattering contributions for the second shell. The DW of the first Nd-O shell was allowed to vary in the multi-shell analysis. Theoretical scattering paths for the fits were calculated using FEFF 8.20 *(1, 4)* and the structure of 11 Å tobermorite *(5)*.

1. Derivation of the EXAFS model

Three different fitting models with the corresponding crystallographic R-factors as obtained from ATHENA/ARTEMIS were used for the F-tests. The R-factor measures the misfit between modeled and experimental Fourier transformed (FT) spectra. The square root of the calculated *R*-factor in ATHENA/ARTEMIS is given here as *R* as suggested elsewhere *(6)*. In order to simplify the discussion, the crystallographic *R*-factors for the fits using models (1) and (2) were labeled as R_1 and the crystallographic *R*-factor for the fits using model (3) was labeled as R_0.

Model (1): Fitting the EXAFS data using a oxygen shell at R + ΔR ~ 2.4 Å and a Si shell at R + ΔR = 3.7 – 3.75 Å.

Model (2): Fitting the EXAFS data using a oxygen shell at R + ΔR ~ 2.4 Å and a Ca shell at R + ΔR = 3.75 – 3.8 Å

Model (3): Fitting the EXAFS data using a oxygen shell at R + ΔR ~ 2.4 Å, a Si shell at R + ΔR = 3.7 – 3.75 and a Ca shell at R + ΔR = 3.75 – 3.8 Å.

The confidence level, α, that a fit that yields a crystallographic *R*-factor R_0 is a better fit than the fit that yields a residual R_1 can be calculated *(6-8)* according to equation (1) :

$$\alpha = P(F > F_{b,n-m,\alpha}) = 1 - I_x\left[\frac{n-m}{2}, \frac{b}{2}\right] \quad (1)$$

,where P represents the probability (in %), $I_x\left[\frac{n-m}{2}, \frac{b}{2}\right]$ is the incomplete regularized beta function, the parameter x is given by $x = \left(\frac{R_0}{R_1}\right)^2$, b is the difference in the degrees of freedom between the fits, which were compared; n is the number of independent data

points as calculated by the Stern`s rule *(9)* and m is the number of fit parameters. Model (3) has 8 independent parameters, that are coordination number, N, (3 parameters), and bond-distances, R, (3 parameters) of the oxygen, Si and Ca shells, DW factor of the oxygen shell (1 parameter) and the correlated E_0 (1 parameter). The models (1) and (2) have each 6 independent parameters, that are N (2 parameters) and R (2 parameters) of the oxygen, Si or Ca shells, DW factor of the oxygen shell (1 parameter) and the correlated E_0 (1 parameter). The maximum number of free parameters describing the signal was estimated by applying the Stern`s rule in the chosen windows in the *k*- and *R* spaces, $N_{Ind.} = 2\Delta k \Delta R/\pi + 2$, where $N_{I.}$ is the number of relevant independent points, Δk is the range of *k*-space being fit, and ΔR is the width of the characteristic frequency in the FT. For this study the fits were performed in the k-range of the Fourier transform of Δk = 1.40 - 10.60 $Å^{-1}$ and the R-range for the fit was ΔR = 1.25 – 4.0. The maximal number of components (or free parameters) describing the EXAFS signal was estimated to be 16.1. In no case did the number of parameters that were varied during fitting procedure exceed the limit given by the Stern`s rule.

The significance of statistical F-tests can be illustrated on the basis of the results for bulk-XAS measurements on Nd doped cement samples equilibrated for 28 and 200 days. Table S2 shows the calculated crystallographic *R*-factors (and the corresponding square root of the *R*-factor in the parentheses), the calculated parameter *x* and the probability for Nd doped cement samples reacted for 28 and 200 days and 26 μmol Nd / g solid phase (CEMHYD-28-26 and CEMHYD-200-26).

For CEMHYD-200-26 the fits yielded crystallographic *R*-factors of R_0 = 0.032 (model (3)), R_1 = 0.092 (models (1) and 0.072 (model (2)) (Table S2). The modelled and measured EXAFS spectra appear very similar (Figure not shown).

Using $n - m = 10.1$, where n is the maximum number of free parameters as calculated by the Stern's rule, m is the number of fit parameters used for the fit with crystallographic *R*-factor R_0 (fit assuming model (3)), and b = 2 (b is the difference in the number of free parameters of the fits being compared, i.e. fits resulting in crystallographic *R*-factors R_0 and R_1) in Eqn. (1) yielded confidences of 94 % and 88 % that, in the case of CEMHYD-200-26 fits assuming model (3) are better than the fits assuming models (1) and (2), respectively.

Table S2. *Calculated crystallographic R-factors, the corresponding square root of the R-factors, the calculated parameter x and the probability for selected Nd doped cement samples reacted for 28 and 200 days and 26 µmol Nd / g solid phase (CEMHYD-28-26 and CEMHYD-200-26) using* $\frac{n-m}{2} = 5.05$ *and* $\frac{b}{2} = 1$.

Sample	Time (days)	Calculated crystallographic *R*-factor			Calculated parameter *x*		Calculated probability	
		model (1) / R_1 [1]	model (2) / R_1	model (3) / R_0	*x(1)*[2]	*x(2)*[3]	*a(1)*[4] *(in %)*	*a(2)*[5] *(in %)*
CEMHYD-200-26	200	0.092 / 0.303	0.072 / 0.268	0.032 / 0.178	0.587	0.664	94	88
CEMHYD-28-26	1	0.074 / 0.272	0.062 / 0.249	0.044 / 0.209	0.768	0.839	74	59

[1] The calculated crystallographic *R*-factors and the corresponding square root of the calculated *R*-factor.

[2] calculated parameter x: $x = \left(\frac{R_0}{R_1} \right)^2$ for model (3) vs. model (1)

[3] calculated parameter x: $x = \left(\frac{R_0}{R_1} \right)^2$ for model (3) vs. model (2)

[4] calculated probability a: $a = 1 - I_x\left[\frac{n-m}{2}, \frac{b}{2} \right]$ for model (3) vs. model (1)

[5] calculated probability a: $a = 1 - I_x\left[\frac{n-m}{2}, \frac{b}{2} \right]$ for model (3) vs. model (2)

For CEMHYD-28-26 fits assuming model (3) yielded confidences of 74 % and 59 %, thus suggesting that the presence of Ca atoms at longer distances does improve the fitting. The confidence that model (3) proves better than models (1) and (2) is high (up to 94%). Additional justification for the presence of Ca and Si can be based on structural arguments. To this aim, the structure of non-doped 11 Å tobermorite was considered and assumed to be a suitable model for poorly ordered C-S-H, e.g. *(10, 11)*.

The layered structure of tobermorite is built up of sheets of seven coordinated Ca polyhedra, which are condensed by wollastonite-type silicate chains on *both* sides. In the tobermorite structure each Ca position is surrounded by both Si and Ca atoms. Because the ionic radius of Nd^{3+} (0.983Å in sixfold coordination) is comparable to that of Ca^{2+} (1.00 Å and 1.07 Å for six- and sevenfold coordination, respectively) *(12)*, Nd could substitute for Ca in the structure of C-S-H phases. Assuming Nd-Ca replacement in the crystal structures of 11 Å tobermorite and as analogues in the amorphous C-S-H structure at Ca positions in the Ca sheets results in Nd - O, Nd - Si and Nd - Ca distances of $R_{Nd\text{-}O}$ ~ 2.37 - 2.46 Å, $R_{Nd\text{-}Si}$ ~ 3.65 - 3.85 Å and $R_{Nd\text{-}Ca}$ ~ 3.7 - 3.9 Å (e.g. structural data were taken from elsewhere *(5)*). Note that lanthanides and trivalent actinides incorporation (e.g. Eu(III) and Cm(III)) into the Ca sheets of C-S-H was already suggested from previous studies *(13, 14)*. The latter finding is in agreement with the proposal that neighbouring Si and Ca atoms have to be included in the fitting and therefore supports

EXAFS data fitting using model (3). Based on the crystallographic data on non-doped crystalline C-S-H (e.g. 11 Å tobermorite) and the results from the F-test, we assume that a model, which includes three shells (i.e., O, Si and Ca atoms) as in model (3), is suitable to reproduce backscattering contributions from neighboring atoms in the structure of C-S-H phases. This model was also applied recently in EXAFS investigation of Eu(III) taken up by amorphous C-S-H phases *(13).*

Results and discussion

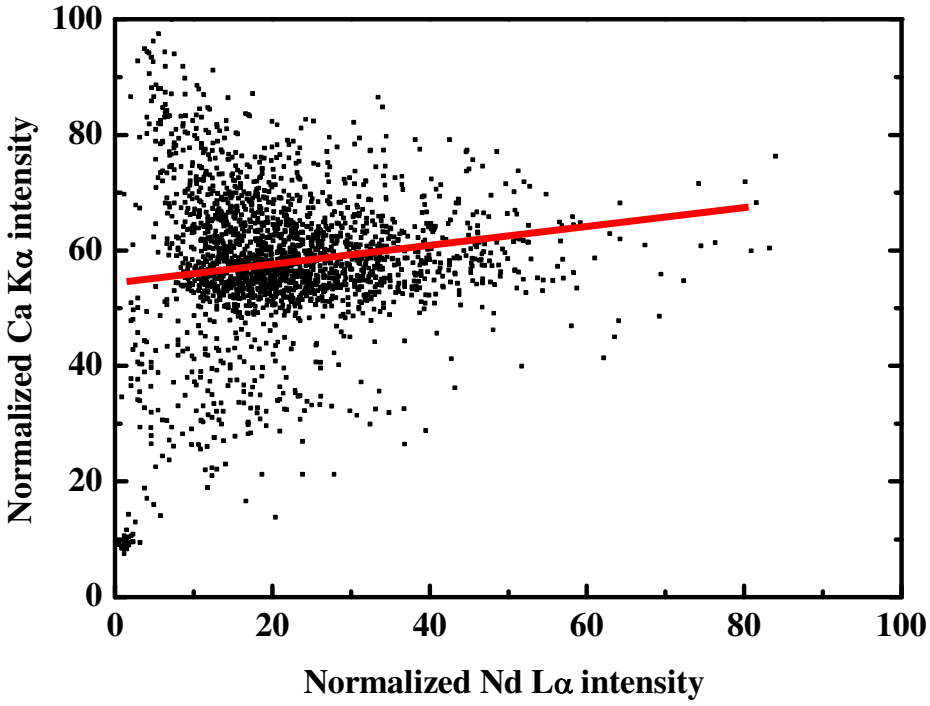

Figure S1: Nd / Ca correlation plot. The correlation plot in Figure S1 depicts the normalized Nd L_α signal versus normalized Ca K_α signal from a 1500 x 700 μm^2 area. The Nd / Ca-correlation lies mainly within the fan defined by these two lines and the plot demonstrate the contrast between Nd and Ca distributions. The line in the figure is a guidetotheeye with slopes 1.6.

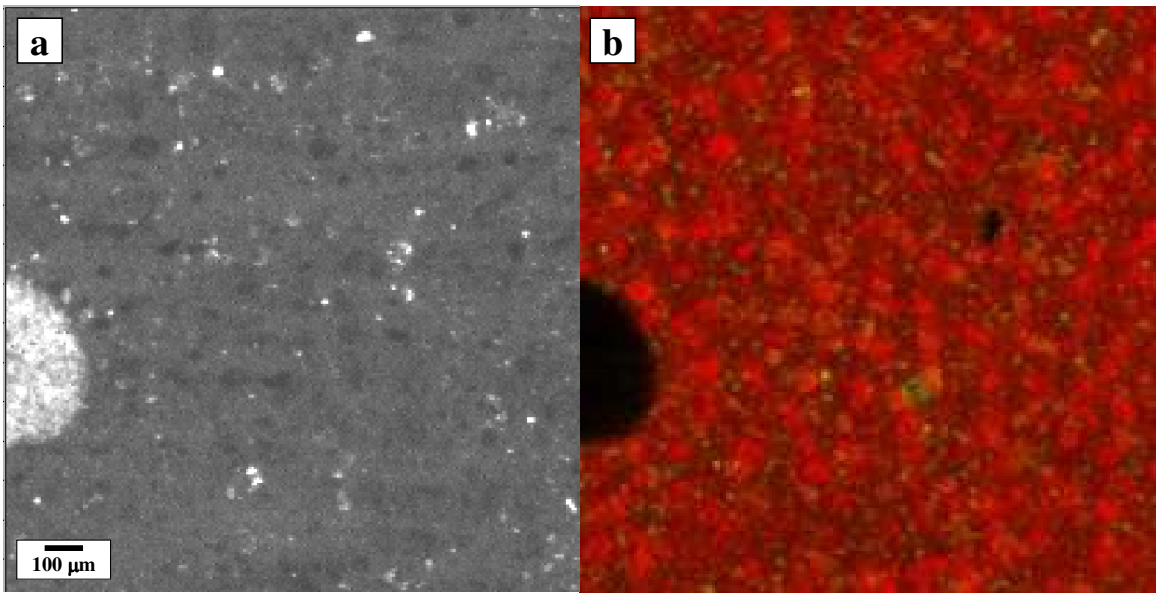

Figure S2: a) Overview map and b) µ-XRF elemental distribution maps of Nd (green) and Ca (red) for the Nd doped HCP samples with a w / c ratio of 0.4, a hydration time of 28 days and a final metal concentration of 26 µmol Nd / g solid phase. The bright spot in Figure S2 stems from silver alloy and was used for orientation.

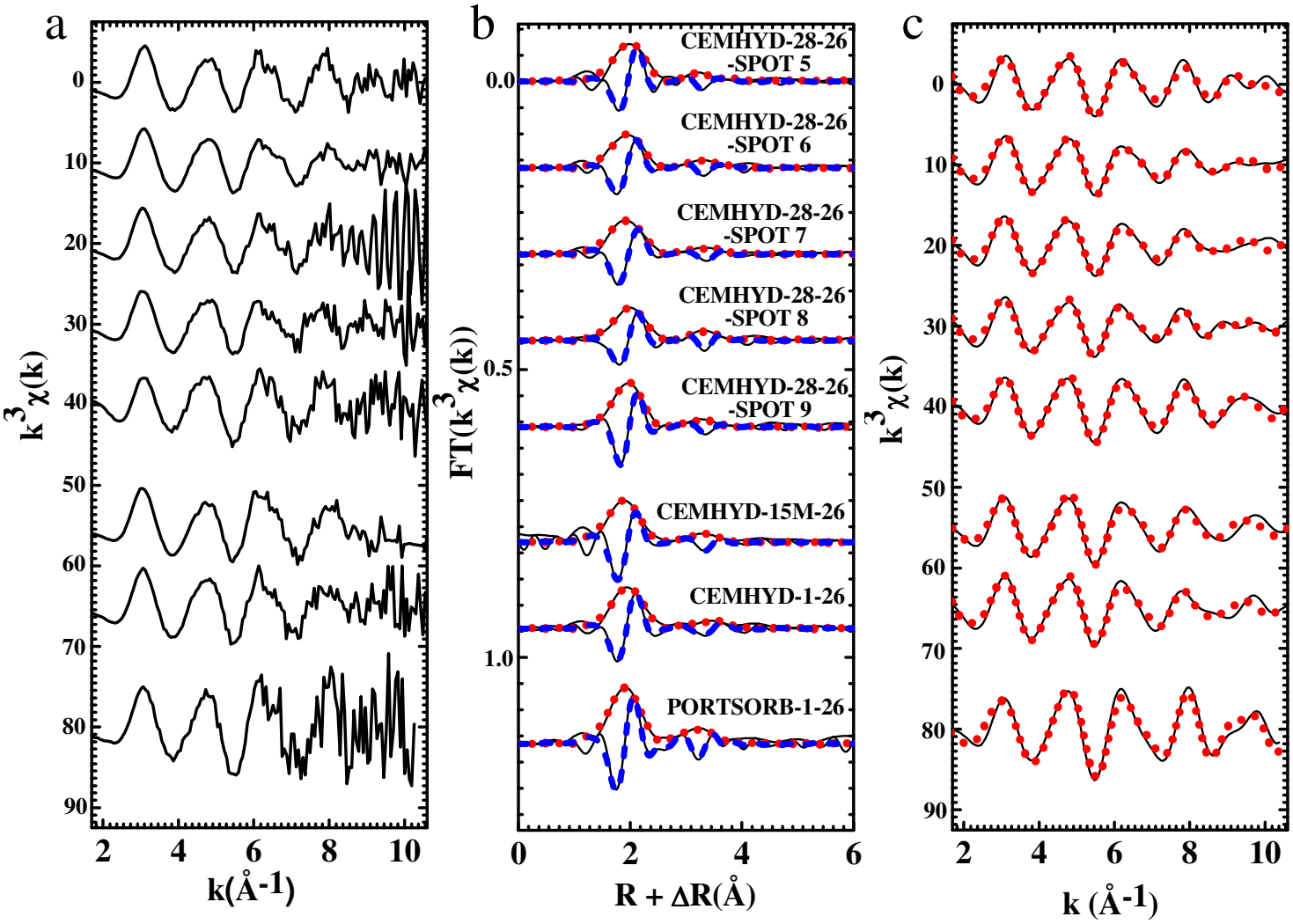
a
b
c
k3χ(k)
k(Å-1)
FT(k3χ(k))
R + ΔR(Å)
k (Å-1)
CEMHYD-28-26 -SPOT 5
CEMHYD-28-26 -SPOT 6
CEMHYD-28-26 -SPOT 7
CEMHYD-28-26 -SPOT 8
CEMHYD-28-26 -SPOT 9
CEMHYD-15M-26
CEMHYD-1-26
PORTSORB-1-26

Figure S3: a) k^3-weighted spectra and b) the corresponding RSFs of experimental (solid line) and fitted (dashed and doted lines for the imaginary and the real part, respectively) Nd L_{III}-edge experimental spectra for μ-EXAFS and bulk-EXAFS measurements of selected Nd doped HCP samples with a water/cement ratio of 0.4, varying reaction time (15 min., 1 day and 28 days) and total metal concentrations of 26 μmol / g solid phase, and Nd doped portlandite; c) k^3-weighted EXAFS function for the Fourier-backtransform spectra obtained from Figure S1b (range: $R + \Delta R = 1.7\text{-}4.0$).

References

(1) Newville, M., EXAFS analysis using FEFF and FEFFIT. *J. Synchrotron Rad.* **2001,** *8* (2), 96-100.

(2) Ravel, B.; Newville, M., ATHENA, ARTEMIS, HEPHAESTUS: data analysis for X-ray absorption spectroscopy using IFEFFIT. *J. Synchrotron Rad.* **2005,** *12*, 537-541.

(3) Allen, P. G.; Bucher, J. J.; Shuh, D. K.; Edelstein, N. M.; Craig, I., Coordination chemistry of trivalent lanthanide and actinide ions in dilute and concentrated chloride solutions. *Inorg. Chem.* **2000,** *39* (3), 595-601.

(4) Ankudinov, A. L.; Rehr, J. J., Theory of the solid-state contribution to the X-ray elastic scattering amplitude. *Phys. Rev. B* **2000,** *62*, 2437-2445.

(5) Merlino, S.; Bonaccorsi, E.; Armbruster, T., The real structure of tobermorite 11Å: normal and anomalous forms, OD character and polytypic modifications. *Eur. J. Mineral.* **2001,** *13*, 577–590.

(6) Downward, L.; Booth, C. H.; Lukens, W. W.; Bridges, F., A variation of the F-test for determining statistical relevance of particular parameters in EXAFS fits. *AIP Conference Proceedings* **2007,** *882* (1), 129-131.

(7) Bacchi, A.; Lamzin, V. S.; Wilson, K. S., A self-validation technique for protein structure refinement: the extended Hamilton test. *Acta Cryst.* **1996,** *D 52* (4), 641-646.

(8) Hamilton, W., Significance tests on the crystallographic R factor. *Acta Cryst.* **1965,** *18* (3), 502-510.

(9) Stern, E. A., Number of relevant independent points in X-ray absorption fine-structure spectra. *Phys. Rev. B* **1993,** *48* (13), 9825-9827.

(10) Richardson, I. G., Tobermorite/jennite- and tobermorite/calcium hydroxide-based models for the structure of C-S-H: applicability to hardened pastes of tricalcium silicate, [beta]-dicalcium silicate, Portland cement, and blends of Portland cement with blast-furnace slag, metakaolin, or silica fume. *Cem. Concr. Res.* **2004,** *34*, 1733-1777.

(11) Taylor, H. F. W., Proposed structure for calcium silicate hydrate gel. *J. Am. Ceram. Soc.* **1986,** *69*, 464-467.

(12) Shannon, R., Revised effective ionic radii and systematic studies of interatomic distances in halides and chalcogenides. *Acta Cryst. A* **1976,** *32* (5), 751-767.

(13) Schlegel, M. L.; Pointeau, I.; Coreau, N.; Reiller, P., Mechanism of europium retention by calcium silicate hydrates: An EXAFS study. *Environ. Sci. Technol.* **2004,** *38* (16), 4423-4431.

(14) Tits, J.; Stumpf, T.; Rabung, T.; Wieland, E.; Fanghanel, T., Uptake of Cm(III) and Eu(III) by calcium silicate hydrates: A solution chemistry and time-resolved laser fluorescence spectroscopy study. *Environ. Sci. Technol.* **2003,** *37* (16), 3568-3573.